https://doi.org/10.5194/egusphere-2025-6144
Preprint. Discussion started: 16 January 2026

Impacts of water advection and CO_2 exchanges on the carbon dioxide removal potential of ocean alkalinity enhancement

Charly A. Moras[1], Matias Saez Moreno[1], Peggy Bartsch[1], Jens Hartmann[1]

[1]Department of Earth System Sciences, University of Hamburg, Hamburg, Germany

Correspondence to: Charly A. Moras (charly.moras@uni-hamburg.de)

Abstract. Ocean alkalinity enhancement is a carbon dioxide removal strategy with high CO_2 uptake potential and rather low cost. Long term modelling studies have focused on this strategy, but most laboratory experiments focus on shorter term with strong advection, which may not be representative of natural systems. Hence, the long-term fate of alkalinity is yet to be addressed. Also, the role of CO_2 ingassing is still largely overlooked. In a new setup, 6-month experiments using solid $Ca(OH)_2$ and $Mg(OH)_2$, and liquid NaOH have been conducted with a constant supply of CO_2. Bottles were either kept stagnant or exposed to slow advection. All experiments revealed lower measured TA compared to expected, but bottles subjected to advection led to nearly twice as much TA generation in some cases and significantly faster CO_2 ingassing rates. This led to a quicker equilibration, decreasing the low CO_2 period, lately identified as a potential threat to living organisms, and a decreased critical alkalinity period (CAP) for $CaCO_3$ formation. Yet, $CaCO_3$ precipitated in most bottles, either as needles with $Ca(OH)_2$ or as "broccolis" with $Mg(OH)_2$. Such broccoli resulted most likely from precipitation on slowly dissolving $Mg(OH)_2$ particles. Once the CAP was over, conditions remained stable with no redissolution of the $CaCO_3$ precipitates. Using NaOH revealed buffering by $Mg(OH)_2$ precipitation, which ultimately redissolved in the bottles exposed to advection. Finally, the bottles exposed to advection represented open ocean conditions with wind speeds of ~3 m s^{-1}, which, given the calm state of the ocean, may serve as a lower threshold for implementation in global models.

Introduction

The increase in atmospheric (CO_2) concentrations since the Industrial Revolution of the 18th century has been identified as the main cause for global climate change (IPCC, 2022). While a strong effort in reducing CO_2 emissions is required, current projections report it insufficient to slow down global warming, with active CO_2 removal from the atmosphere the only solution (Hausfather, 2025). Among the different carbon dioxide removal (CDR) strategies, Ocean Alkalinity Enhancement (OAE) has gained momentum over the past decade as it may have one of the highest carbon capture potentials. Through the spreading of alkaline materials in coastal areas or in the open ocean for example, the increase in total alkalinity (TA) allows for more CO_2 to be captured by the ocean (Kheshgi, 1995). However, understanding whether added alkalinity remains in the surface ocean is yet to be fully addressed, and especially whether such alkalinity remains stable long enough to allow for CO_2 equilibration. Some issues, such as calcium carbonate ($CaCO_3$) precipitation, have been identified recently and may lead to decreased CDR potential or even CO_2 emissions from the ocean itself (Moras et al., 2022).

https://doi.org/10.5194/egusphere-2025-6144
Preprint. Discussion started: 16 January 2026

When TA is increased by about 500 µmol kg^{-1} using solid feedstocks such as $Ca(OH)_2$ and $Mg(OH)_2$, the increase in alkalinity and the presence of solid surface area enhance $CaCO_3$ precipitation (Hartmann et al., 2023; Moras et al., 2022; Moras et al., 2024; Suitner et al., 2024). During the dissolution of the powdered mineral, the micro-environment formed around the alkaline particles likely reaches very high saturation levels of $CaCO_3$ (Ω_A), where it may precipitate in the form of aragonite (Moras, 2023). Aragonite precipitation may occur homogeneously or heterogeneously on particles, using the yet to be dissolved particles as nuclei (Marion et al., 2009). Once precipitation starts, it enters a runaway pattern where the precipitation speed increases, sometimes reaching TA values lower than the starting conditions (Moras et al., 2022). Under some circumstances, the presence of inhibitors such as magnesium (Mg^{2+}) or dissolved organic matter may delay or decrease the precipitation rate (Chave and Suess, 1970; Pan et al., 2021). Hence, one could suggest that $Mg(OH)_2$ may be a more favourable mineral than $Ca(OH)_2$, as the Mg^{2+} released from $Mg(OH)_2$ dissolution could inhibit $CaCO_3$, and $Ca(OH)_2$ may allow for early nucleation due to the lattice compatibility of $CaCO_3$ for such particles (Moras et al., 2022; Pan et al., 2021; Tang et al., 2020). The nucleation time depends on the persistence of micro-environments and the lattice compatibility between the alkaline mineral surface area and $CaCO_3$. The duration of the critical alkalinity period, later referred to as CAP, dictates the stability of the added alkalinity. When this period is shortened during dilution or quicker dissolution, for example, the risk for $CaCO_3$ precipitation decreases.

To understand such mechanisms, laboratory experiments have been run in a variety of settings, usually for short periods of time, and mostly relying on the use of stir bars in closed reaction vessels. While these settings allow for better comparison between the various dissolution of alkaline minerals, and possible precipitation of $CaCO_3$, they usually omit the role of CO_2 ingassing on the stability of alkalinity. They also provide results for a water perturbation much more important than what would occur in a natural setting. In a new approach, the dissolution of $Ca(OH)_2$ and $Mg(OH)_2$ in natural seawater were addressed both in static and rotating reaction vessels. The rotation speed was selected to allow for vertical diffusion of alkaline material without inducing surface tension breaking, and each vessel was kept open to the air with a constant and identical influx of ambient air. Carbonate chemistry was monitored throughout, particle analyses were conducted at the end of the experiments, and gas velocities for CO_2 and equivalent open ocean wind speeds were derived.

Material and methods

Overview and revolutions per minute (RPM) selection

The experiments were run over 6 months, with two distinct experimental setups. The first one consisted of 42 bottles kept at room temperature and opened to the air on a table, representing the stable conditions. Another set of 42 bottles was kept at room temperature and opened to the air on a shaking table, Edmund Bühler 30 SM C, set to a circular motion at 125RPM. The choice of RPM was the maximum speed allowing for enough movement to create a vertical mixing through diffusion while avoiding any spilling from the bottles. The 125RPM was chosen following side experiments consisting of adding powdered Phenolphthalein dye to seawater in a 1L Schott bottle. The dye changes from a colourless powder to a bright

https://doi.org/10.5194/egusphere-2025-6144
Preprint. Discussion started: 16 January 2026

pinkish colour when dissolved in solutions of pH higher than 8. Such experiments showed that below 80RPM, the vertical mixing of the dye was insufficient, with most of the dye sinking and remaining at the bottom of the bottle. Past 130RPM, the seawater contained in the bottles was reaching the edge of the bottle and was deemed too high of a risk of spilling. Therefore, the suitable motion speed was selected slightly lower, with 125RPM providing suitable particle resuspension yet avoiding water overflow.

Experimental setup

The bottles were cleaned in a 3-step process. They were first soaked overnight in a 1% solution of NaOH with dishwashing tablets. The next day, the bottles were rinsed with tap water three times and soaked overnight in a 0.5% solution of HCl. Finally, all bottles were rinsed with tap water and MilliQ (18.2 MΩ) three times each, before being dried overnight in an oven at 60 °C. About 90L of Indian Ocean natural seawater was collected ~ 400km southeast of Sri Lanka (2°59.995'N, 77°59.997'E) and stored in five 18L borosilicate 3.3 bottles in the dark in the fridge at 4 °C. The total amount of seawater was sterile filtered using a Whatman Polycap 36 AS encapsulated filter with a 0.2 µm pore size. The seawater was stored in a cleaned and MilliQ rinsed 210 L PP rainwater tank (Garantia rainwater green round barrel). The seawater was bubbled for a week using MilliQ saturated ambient air as per Moras et al. (2023) to allow for the whole content of the tank to be equilibrated with air pCO_2.

One major issue when it comes to open bottles is evaporation. In order to decrease evaporation, MilliQ saturated air was provided in all bottles using a similar process to the one described above for the seawater. Air was pumped into MilliQ contained in a sealed 1L Schott bottle. Once the air was bubbled through the MilliQ, it was carried over into plastic air flow dividers similar to those used for aquariums. Each of the tubing were placed in the headspace of each of the bottles and was maintained using binder clips connected to the bottle neck. The air was not allowed to bubble the seawater directly but ensured that each of the bottles' headspaces was consistently provided with the same freshly MilliQ-saturated air, allowing for easier comparison of results from bottles as they were all exposed to the same conditions. Each bottle was also weighed regularly (every 2-3 days) to ensure that evaporation was not too important. When a difference in weight was with 5-10% difference after these 2-3 days, a slight addition of fresh MilliQ was performed to compensate for the slight evaporation. Another issue that was raised before the start of the experiments was the risk of organisms growing in the bottles. In order to prevent or at least decrease such growth, two germicidal UV lamps with ozone light of 254nm were mounted on top of the setup and placed so that all bottles were exposed to the UV lights. These lamps were automatically switched on for an hour twice a week in the middle of the night, allowing for a long enough exposure to prevent organisms' growth.

TA manipulations and sampling procedure

Each of the cleaned 84 bottles was filled with ~900g of sterile filtered seawater. Two sets of 42-bottle experiments consisted of control bottles filled only with sterile filtered seawater, and TA-enhanced bottles, using either $Ca(OH)_2$ powder, $Mg(OH)_2$ powder, or 1M NaOH solution. The enhanced alkalinity ranged from +100 µmol kg^{-1} to +600 µmol kg^{-1} with 100 µmol kg^{-1}

https://doi.org/10.5194/egusphere-2025-6144
Preprint. Discussion started: 16 January 2026

TA increments for both alkaline powders, and only one set of +600 µmol kg^{-1} using NaOH. Every manipulation was conducted in triplicate, leading to 3 control bottles, 18 TA enhanced bottles using $Ca(OH)_2$, 18 TA enhanced bottles using $Mg(OH)_2$, and 3 TA enhanced bottles using NaOH (one bottle was lost for the 125RPM treatment from day 6 onwards and one was lost for the 0RPM treatment from day 108 bottles, data reported are the average of the two remaining replicates). Both the static and moving treatments consisted of the same 42 bottles set to allow for comparison.

The alkaline powders used are reagent-grade $Ca(OH)_2$ and $Mg(OH)_2$, and the NaOH pellets used to make the 1M NaOH solution were reagent-grade, all obtained from Carl Roth. The $Ca(OH)_2$ and $Mg(OH)_2$ powders were sieved through a 32 µm aluminium steel sieve to allow for direct comparison. Both powders were dried overnight at 60 °C. The NaOH solution was added using an Eppendorf Research Plus 1000 pipette, while the $Ca(OH)_2$ and $Mg(OH)_2$ powder were weighed on a weighing paper using a Kern ABT 120-5DNM (± 0.01mg) balance. Overall, the weighing uncertainty led to an offset between the targeted and estimated TA of less than 1%.

The pH, temperature and conductivity of each sample were measured before manipulation, after 1-, 3- and 6-days following alkalinity addition. Thereafter, measurements took place twice a week for the first 2 months and once a week afterwards. TA and DIC samples were taken before manipulation, at day 1, 3 and 7, and monthly afterwards. Seawater was sampled using a peristaltic pump connected to a 0.2 µm filter from Sartorius. 24mL borosilicate 3.3 TOC vials from Shimadzu were smoothly filled from the bottom with a 14-gauge needle and allowed to overflow by at least half of their volume. The vials were then closed with screw caps with silicone red/PTFE white double-layered septa without headspace. TA samples were collected right after DIC samples, with about 20mL of sample being collected in 100mL PP bottles. The TA bottles were closed tightly to prevent any evaporation, and both TA and DIC samples were stored in the fridge in the dark until analysis.

Carbonate chemistry measurements and calculations

pH and conductivity were measured using a Multiparameter pocket measuring device, MultiLine Multi 3630 IDS from WTW, using a SenTix 940 pH probe and a WTW TetraCon 925 conductivity probe. The pH probe was calibrated weekly using NIST standards and converted to the pH on the total scale (pH_T) as per Badocco et al. (2021). The conductivity was calibrated before the first measurement to determine the starting salinity of the seawater. The salinity was estimated at 35.346 ±0.077 on the practical salinity scale of 1978 (Lewis and Perkin, 1981). The TA was determined with a potentiometric titration with a 888 Titrando connected to a 814 USB Sample Processor from Metrohm, with a 0.02M HCl solution as the titrant. The titrant ionic strength was adjusted to 0.72 mol kg^{-1} by NaCl addition, corresponding to a salinity of 35 (Dickson et al., 2007). The raw TA values were corrected against certified reference materials (CRM #187) from Dickson (2010). The overall instrument uncertainty was estimated at 0.1% via error propagation of all CRM measurements. DIC analyses were conducted on a Shimadzu TOC-L/CPH analyser calibrated using CRM (#207). Samples were injected into the reactor filled with fresh 25% H_3PO_4, and DIC was carried with CO_2-free air. The overall instrument uncertainty was also determined via error propagation of all CRM measurements and estimated at 3.5%.

https://doi.org/10.5194/egusphere-2025-6144
Preprint. Discussion started: 16 January 2026

During the 6-month experiment, atmospheric CO_2 concentration, temperature and humidity were recorded every 15 minutes with a HOBO MX1102A CO_2 logger to control for any spike in atmospheric CO_2 and/or temperature. The pCO_2 logger was automatically calibrated to 400 ppm (as per manufacturer recommendations) by placing the logger in open air until a stable reading was recorded. Such calibration would not allow for accurate pCO_2 measurement but rather control whether spikes in pCO_2 occurred during the experiments. Overall, atmospheric pCO_2 (437.7 ±34.6 ppm) only varied by less than 1% throughout the experiment, and the average temperature was recorded at 24.6 ±1.4 °C (later rounded to 25 °C for further processing). To compensate for such atmospheric pCO_2 measurement uncertainty, the estimated pCO_2 from the control batches will be used as the background concentration. To do so, using TA, DIC, salinity and temperature measurements, and using the K1 and K2 dissociation constants from Schockman and Byrne (2021), KSO_4 dissociation constant from Dickson (1990), KF dissociation constant from Perez and Fraga (1987) and the borate-to-salinity ratio from Lee et al. (2010), the sample pCO_2 could be determined, as well as other carbonate chemistry parameters such as Ω_A.

Secondary mineral formation was observed in all incubations and was suspected to occur on the surface of added material, i.e., $Ca(OH)_2$ and $Mg(OH)_2$. Scanning electron microscopy (SEM) analyses were conducted on a tabletop Hitachi TM4000 II, connected to a Bruker QUANTAX energy-dispersive x-ray spectroscopy (EDS). At the end of the experiments, about 20mL of remaining water was collected on Whatman polycarbonate Nuclepore filters (0.2 µm) from the higher treatments to ensure a significant amount of sample. The samples were then rinsed with MilliQ before being dried at 60 °C overnight. The filters were then mounted on an aluminium filter holder using double-sided carbon sticky tabs. The small remaining volume of the higher treatments using $Mg(OH)_2$ was also collected for Ca^{2+} and Mg^{2+} analyses, to decipher whether undissolved $Mg(OH)_2$ could have been used for $CaCO_3$ precipitation. The remaining volume was weighed and filtered on a Whatman polycarbonate Nuclepore filter (0.2 µm) and placed into a 50mL Falcon tube to dry overnight. The incubation bottle was then rinsed three times with ~15mL of 3% Suprapure nitric acid to try and remove any precipitate on the wall. The acid was then transferred to the Falcon tube with the filter to dissolve any collected particles before being topped up to 50mL. Concentrations of Ca and Mg were analysed via Flame Atomic Absorption Spectroscopy (F-AAS) on a Thermo Fisher Solaar S Series.

Quality control was conducted using the TA, DIC and pH_T data from each set. The DIC measurements from months 1 and 2 were likely underestimated, while the DIC measurements from month 6 were likely overestimated (Figure A 1). While little to no changes were observed with TA and pH_T measurements, these changes in DIC suggested a measurement issue, which coincided with issues with the temperature control in the laboratory where analyses were conducted. Therefore, a comparison of the offset between measured DIC and estimated DIC from measured TA and pH_T were conducted. The boxplot analysis revealed that the months 1 and 2 DIC measurements were significantly lower than the average offset, while the month 6 DIC measurements were significantly higher. Therefore, the DIC concentration for these three points was corrected using the average offset of all measurements. Initial DIC values of the 1-month dataset were overestimated by ~101 ±5 µmol kg^{-1}, those of the 2-month dataset were overestimated by ~47 ±3 µmol kg^{-1}, and those of the 6-month dataset

https://doi.org/10.5194/egusphere-2025-6144
Preprint. Discussion started: 16 January 2026

were underestimated by ~67 ±4 µmol kg^{-1}. The TA dataset from day 6 of the 125RPM experiments was lost during analysis. The TA datapoint was created assuming linear changes between day 3 and 35.

Results

Differences between expected and measured alkalinity

Alkalinity additions for each experiment were performed identically with ΔTA targets varying from +100 to +600 µmol kg^{-1}. In all experiments, the expected maximum ΔTA was not reached, but positive ΔTA were observed at day 1. Within these first 24 hours, stark differences emerged between the material used and the advection. The $\%TA_{realised}$, i.e., net measured ΔTA in µmol kg^{-1} divided by the targeted ΔTA in µmol kg^{-1}, was significantly lower in bottles with no advection (Figure 1). Bottles exposed to motion led to a $\%TA_{realised}$ 2.5 ±1.0 and 4.3 ±2.1 times higher than the static ones for $Ca(OH)_2$ and $Mg(OH)_2$, respectively.

In all cases, the $\%TA_{realised}$ decreased with increasing ΔTA targets. Using $Mg(OH)_2$, the $\%TA_{realised}$ appears to consistently decrease, regardless of the advection speed, while using $Ca(OH)_2$, the loss in $\%TA_{realised}$ quickly decreases with advection and leads to converging values for the 0 and 125RPM scenarios at ΔTA targets of 500 and 600 µmol kg^{-1}. It appears that the measured TA generation from $Mg(OH)_2$ without advection remains mostly lower than using $Ca(OH)_2$, with values varying between 3-18% with $Mg(OH)_2$, and 3-30% with $Ca(OH)_2$ compared to the expected TA increase. However, when exposed to advection, the TA generation of $Mg(OH)_2$ was mostly higher than when using $Ca(OH)_2$, and the loss in efficiency is not as pronounced compared to those of $Ca(OH)_2$. Advection led to a $\%TA_{realised}$ varying between 10-55% using $Ca(OH)_2$, and between 29-58% using $Mg(OH)_2$.

https://doi.org/10.5194/egusphere-2025-6144
Preprint. Discussion started: 16 January 2026

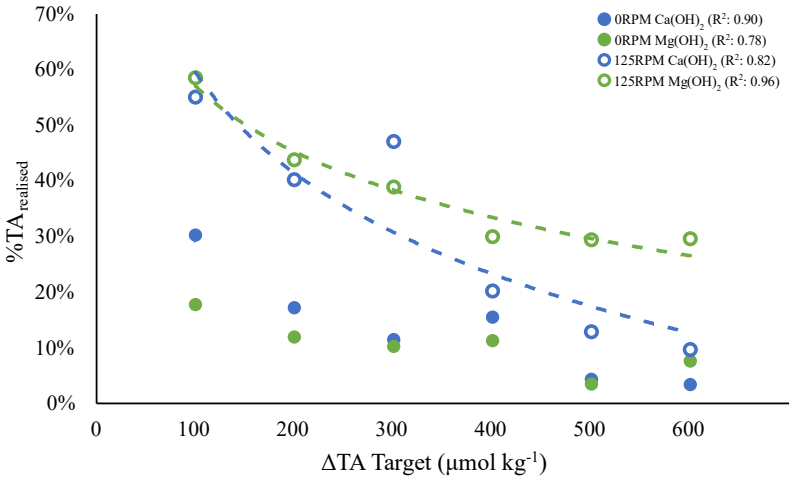

Figure 1: %TA$_{realised}$ (ΔTA measured) after 1 day as a function of the ΔTA target (in µmol kg^{-1}). Each point represents the average of each triplicate, with blue markers representing the Ca(OH)$_2$ treatments and the green markers representing the Mg(OH)$_2$ treatments. Dotted lines represent logarithmic fits of the 0RPM treatments while the dashed lines represent the logarithmic fits of the 125RPM treatments. Corresponding R^2 are provided in the legend.

Long-term stability of alkalinity

In most cases, the TA measured at 24h was higher than the remaining 6 months data. Two clear patterns emerged between the 0RPM and 125RPM incubations (Figure 2). The absence of advection mostly led to a negative ΔTA overtime. With Ca(OH)$_2$, a clear loss in TA followed the 500 and 600 µmol kg^{-1} additions, where after ~2 months, nearly 100 and 180 µmol kg^{-1} were lost, respectively. However, smaller additions led to slight changes in ΔTA but without a clear gain or loss over time. Using Mg(OH)$_2$ led to a clear decrease in alkalinity over time, with a higher loss in alkalinity with higher material addition. After a month, the two higher additions led to a loss in TA of 150-180 µmol kg^{-1}. The two medium additions led to a loss in TA of about 50 µmol kg^{-1}, while lower additions led to losses around 10-20 µmol kg^{-1}.

However, once exposed to advection, the ΔTA is mostly positive in all cases, except for the 600 µmol kg^{-1} addition with Ca(OH)$_2$. With additions of 100, 200 and 300 µmol kg^{-1} with Ca(OH)$_2$, ΔTA increased by ~50, ~80, and ~130 µmol kg^{-1}, respectively, and remained relatively stable over time. The 400 and 500 µmol kg^{-1} additions did not generate more TA than the lower additions, with a starting ΔTA decreasing over time, from ~80 to 40 µmol kg^{-1} for the 400 µmol kg^{-1} target, and from ~60 to a slightly negative ΔTA for the 500 µmol kg^{-1}. Finally, the 600 µmol kg^{-1} treatment led to the lowest ΔTA increase of about 50 µmol kg^{-1} before decreasing consistently over 6 months down to about -140 µmol kg^{-1}. Conversely, the Mg(OH)$_2$ treatments led to increasing ΔTA with increasing additions, and positive over the 6-month experiment. The +100, +200 and +300 µmol kg^{-1} treatments saw an increase over time in ΔTA despite a rather stable phase over the first week. The +400 and +500 treatments did not lead to a secondary increase in alkalinity but stayed stable over the 6-month experiments,

https://doi.org/10.5194/egusphere-2025-6144
Preprint. Discussion started: 16 January 2026

following a peak in ΔTA on day 1 and sight loss until day 3. Finally, the higher $Mg(OH)_2$ treatment saw the highest drop in ΔTA over time, from nearly 180 µmol kg^{-1} on day 1, to about 100 µmol kg^{-1} after 2 months, before remaining stable until the end of the experiment.

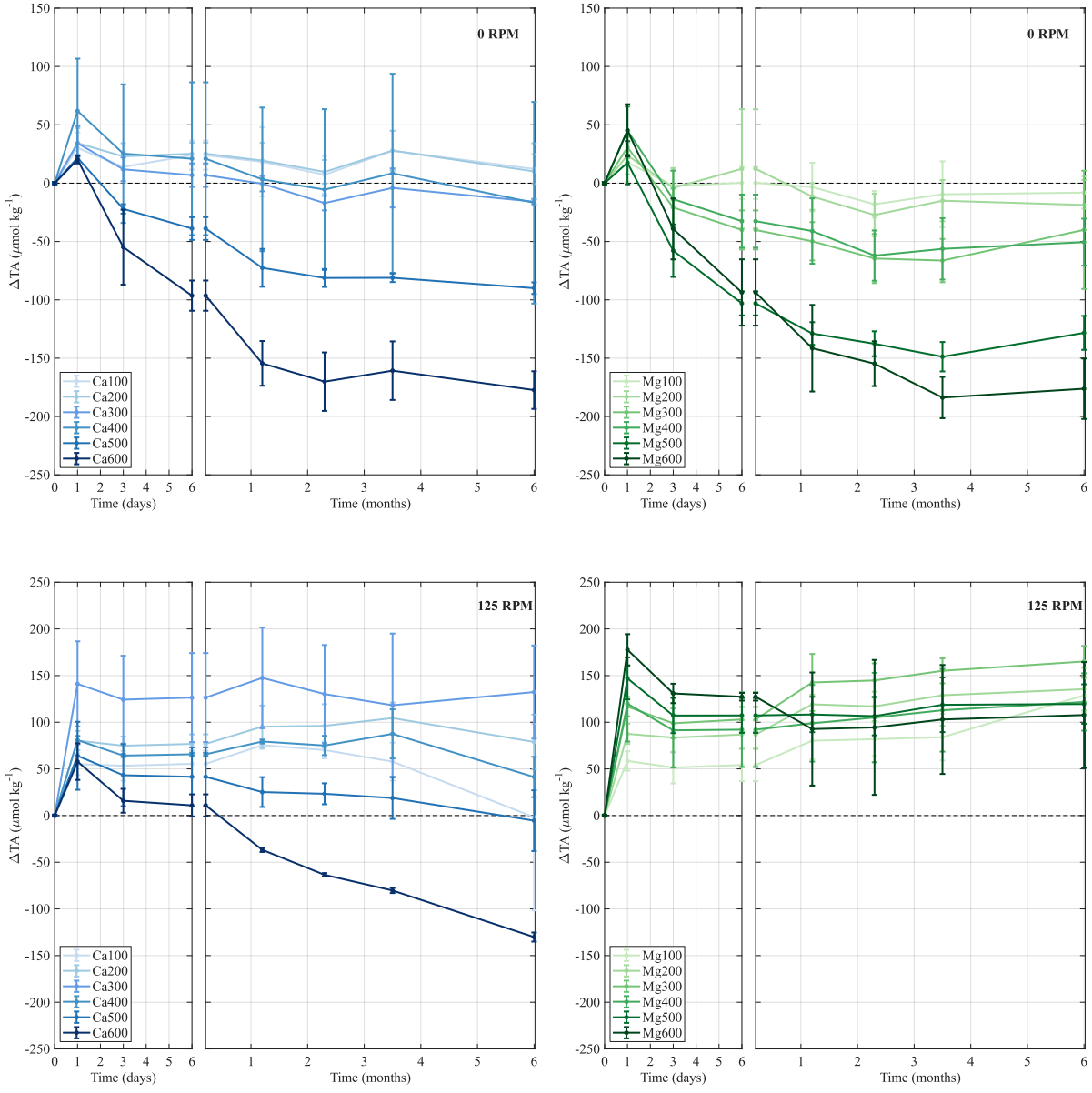

Figure 2: Changes in TA (ΔTA) as a function of time and expressed in µmol kg^{-1}. The 0RPM experiments are represented in the top two tiles, while the 125RPM experiments are represented in the bottom two tiles. $Ca(OH)_2$ additions are represented in blue and $Mg(OH)_2$ additions in green, with the shades representing the amount added, i.e., the darker the shade, the higher alkaline

https://doi.org/10.5194/egusphere-2025-6144
Preprint. Discussion started: 16 January 2026

material addition. Each point represents the average of triplicates, with ranges representing the uncertainty based on the standard deviation of these three measurements.

Effects of advection on pCO_2 changes

Following alkalinity additions, clear drops in the water pCO_2 were observed in all experiments. In most cases, the higher the targeted ΔTA led to the lower the pCO_2 value, except for the 0RPM $Ca(OH)_2$ experiment, where the lower pCO_2 was observed in the +400 µmol kg^{-1} experiment. In the 0RPM experiments, the lowest pCO_2 recorded was 250-280 µatm in the $Ca(OH)_2$ and $Mg(OH)_2$ experiments, respectively. With $Ca(OH)_2$, pCO_2 slowly increased over 1 month until reaching values similar to the control incubations. Over the next 5 months, pCO_2 slightly varied, mostly following the control batch concentrations. In the case of $Mg(OH)_2$ at 0RPM, pCO_2 remained mostly stable or increased slightly during the first week and eventually reached control values after 2 months of experiment. In the 125RPM experiment, the sharp drop in pCO_2 following alkaline material addition was quickly met with a sharp increase in pCO_2 the following days. In the case of $Ca(OH)_2$, after only 24h were the pCO_2 values were back to concentrations similar to the control incubations. The $Mg(OH)_2$ incubations' pCO_2 also quickly bounced back, but reached control values only after 6 days. In both cases, the pCO_2 remained rather consistent over the following 6 months, with variations following the same patterns as for the control incubations.

https://doi.org/10.5194/egusphere-2025-6144
Preprint. Discussion started: 16 January 2026

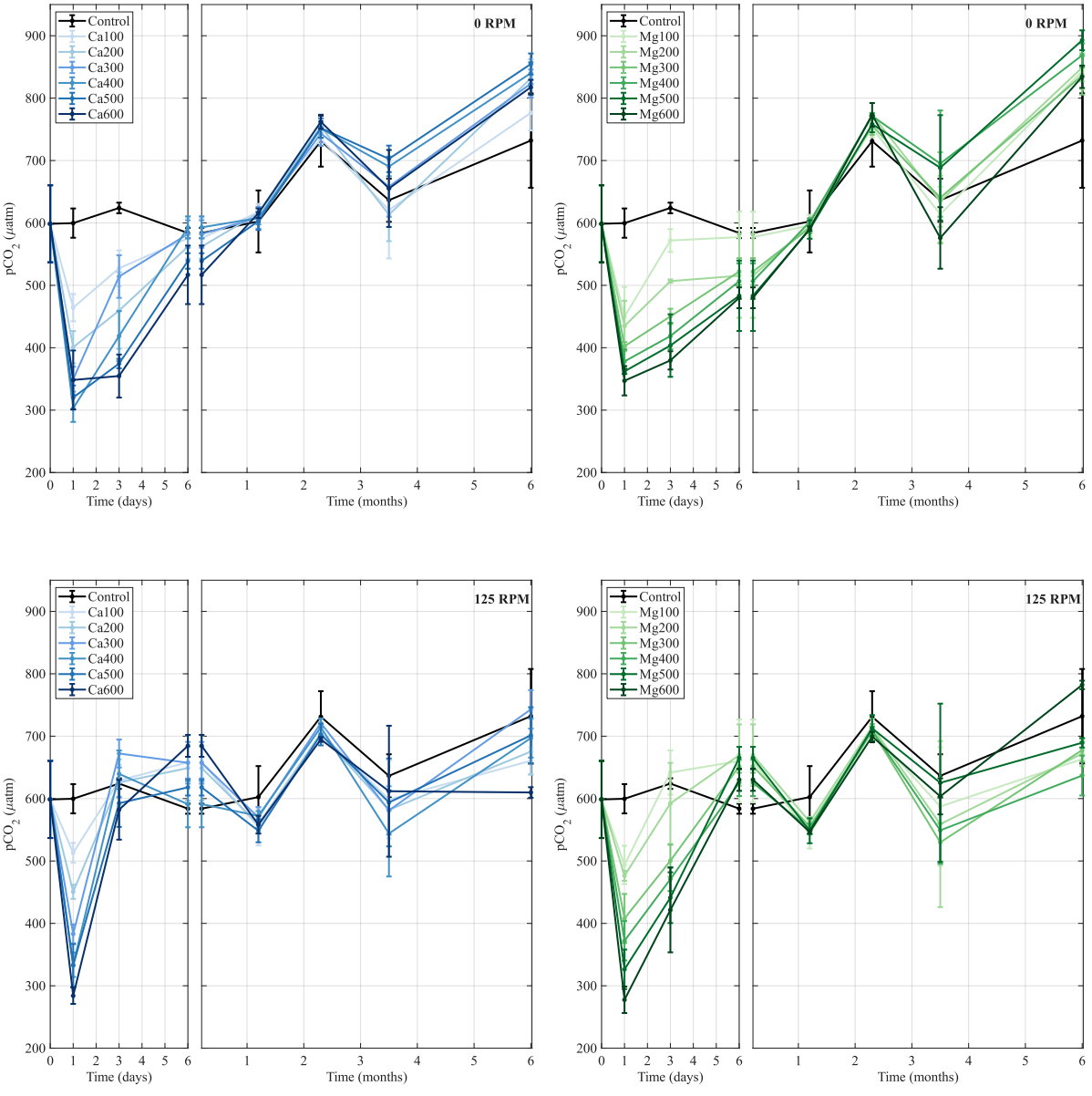

Figure 3: Estimated pCO_2 values from measured TA and DIC and reported in µatm, as a function of time. The 0RPM experiments are represented in the top two tiles, while the 125RPM experiments are represented in the bottom two tiles. $Ca(OH)_2$ additions are represented in blue and $Mg(OH)_2$ additions in green, with the shades representing the amount added, i.e., the darker the shade, the higher alkaline material addition. Each point represents the average of triplicates, with ranges representing the uncertainty based on the standard deviation of these three measurements.

https://doi.org/10.5194/egusphere-2025-6144
Preprint. Discussion started: 16 January 2026

NaOH experiments and differing patterns

The NaOH experiments revealed similar patterns to those from the $Ca(OH)_2$ and $Mg(OH)_2$. While both setups are meant to be identical, a clear difference emerges regarding the ΔTA. At 0RPM, ΔTA only reaches about 278 µmol kg^{-1} within 24h and peaks at 337 µmol kg^{-1} after three days, corresponding to about 56% of the expected TA. The 125RPM experiments quickly reach about 552 µmol kg^{-1} after one day, before reaching up to 598 µmol kg^{-1} after 3 months, corresponding to about 100% of expected TA. DIC followed a similar pattern in both cases, but the final ΔDIC was about half in the 0RPM experiments compared to the 125RPM. Also, while ΔDIC was positive throughout the experiment at 125RPM, the 0RPM experiment first showed a decline at day 1 of about 17 µmol kg^{-1} before consistently increasing until the end of the experiment. pCO_2 decreased after NaOH addition down to similar levels for both 0 and 125RPM experiments, i.e., 209 and 167 µatm, respectively. The increase that followed was quicker in the 125RPM experiments, where, after only 6 days, pCO_2 was similar to the control one, while it took at least one month for pCO_2 to be similar to the control with 0RPM.

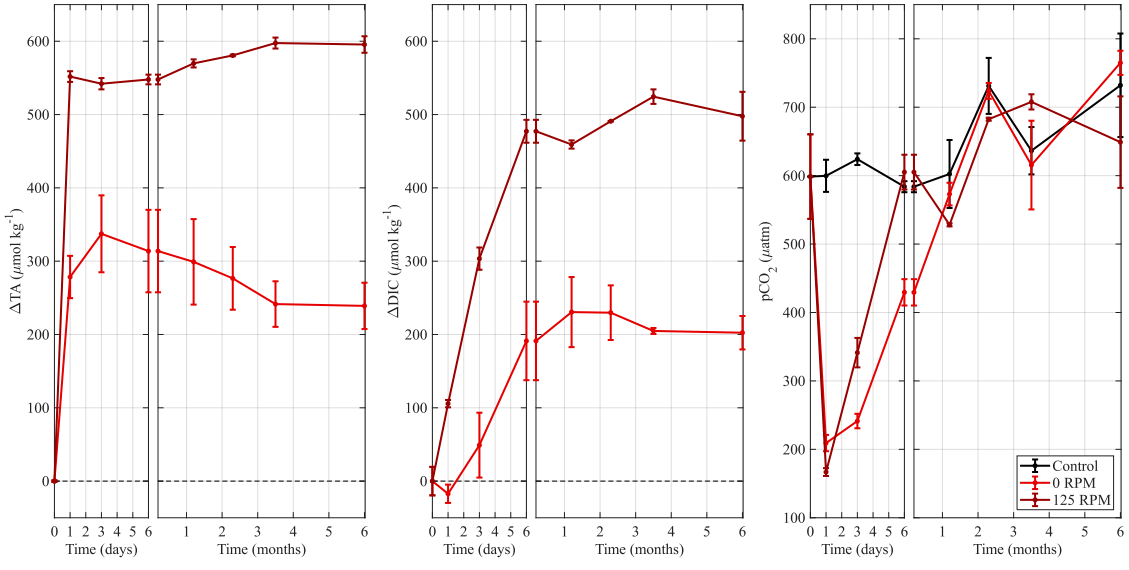

Figure 4: TA, DIC and pCO_2 changes as a function of time for the NaOH experiments. The black colour represents the control experiment, the lighter red colour represents the 0RPM experiments, and the darker red colour represents the 125RPM experiments.

Particulate analysis and scanning electron microscopy

Particulate analysis was conducted using the precipitates from the highest additions of $Mg(OH)_2$, i.e., +600 µmol kg^{-1}, at both 0 and 125RPM, to allow for a strong enough signal and decipher whether $Mg(OH)_2$ particles are used as surface area

https://doi.org/10.5194/egusphere-2025-6144
Preprint. Discussion started: 16 January 2026

for $CaCO_3$ precipitation. The sample for the third replicate of the 0RPM $Mg(OH)_2$ treatment was lost during analysis, and not all interpretations could be computed in Table 1 for this sample in particular. Using the total measured TA loss (Meas. TA_{loss}) and the estimated maximum ΔTA reached from the amount of feedstock added in each bottle, an estimated maximum TA_{loss} term (Max. TA_{loss}) can be calculated. The data support the TA patterns observed in Figure 2, where the experiments run at 0RPM clearly show a stronger Max. TA_{loss} of about 194 µmol kg^{-1} than those run at 125RPM. The results obtained from F-AAS correlate with such observations, where the measured concentrations of particulate Ca^{2+} and Mg^{2+} are about 7.2 and 0.4 mg L^{-1} lower in the 125RPM, respectively. Using the Max. TA_{loss}, an estimated particulate Ca^{2+} concentration can be determined (estimated Ca^{2+}). On average, 62.7% ±4.4% and 58.2% ±5.2% of the estimated Ca^{2+} is explained by the measured Ca^{2+}, for 0 and 125RPM, respectively. Finally, another major difference emerges from the measurements of Mg^{2+}, where the 0RPM has nearly twice as much Mg^{2+} as the 125RPM. On average, the particles analysed from the 0RPM experiments are composed of magnesium by 3.8% ±0.4% while it is slightly less for the particles from the 125RPM experiments, i.e., 3.0% ±0.3%.

Table 1: Comparison of expected and measured changes in TA from the amount of material added, measured TA loss and estimated total loss assuming full dissolution. Ca^{2+} loss from the water column estimated from changes in TA and measured Ca^{2+} and Mg^{2+} from precipitates in the 0 and 125RPM experiments with the highest addition of $Mg(OH)_2$. A ratio between measured Ca^{2+} and estimated Ca^{2+} is also provided.

Sample replicate		Max. ΔTA estimated (µmol kg^{-1})	Meas. TA_{loss} (µmol kg^{-1})	Max. TA_{loss} (µmol kg^{-1})	Estimated Ca^{2+} (in mg L^{-1})	Measured Ca^{2+} | Mg^{2+} (in mg L^{-1})	%meas vs est.
0RPM	1	596.6	237.2	769.1	38.5	25.3 | 1.1	65.8%
	2	601.5	231.9	801.1	40.1	23.9 | 0.9	59.6%
	3	598.1	238.2	814.5	40.7	LOST	LOST
125RPM	1	605.2	177.6	599.2	30.0	16.8 | 0.5	56.1%
	2	598.8	258.8	665.5	33.3	18.1 | 0.5	54.4%
	3	600.6	96.9	537.7	26.9	17.2 | 0.6	64.1%

For the same incubations, as well as the higher treatments of the $Ca(OH)_2$ experiments at 0 and 125RPM, samples for SEM analysis were taken and analysed. Precipitate analyses revealed clear and strong signals for calcium, oxygen and carbon in all samples, with traces of magnesium, strontium, sodium and chloride, i.e., <1% on average compared to the above-mentioned elements. While no clear difference in the composition of precipitates was observed, the morphology was clearly different. Precipitates from the $Ca(OH)_2$ experiments mostly appeared needle-like, as shown in Figure 5. A major difference emerges when comparing those with the precipitates from the $Mg(OH)_2$ experiments. In both cases, the morphology of the

https://doi.org/10.5194/egusphere-2025-6144
Preprint. Discussion started: 16 January 2026

crystals was clearly different, with crystals appearing denser and displaying a broccoli-like structure. While it is harder to identify a single crystal, these precipitates were mostly bigger than those observed in the $Ca(OH)_2$ experiments (Figure 5).

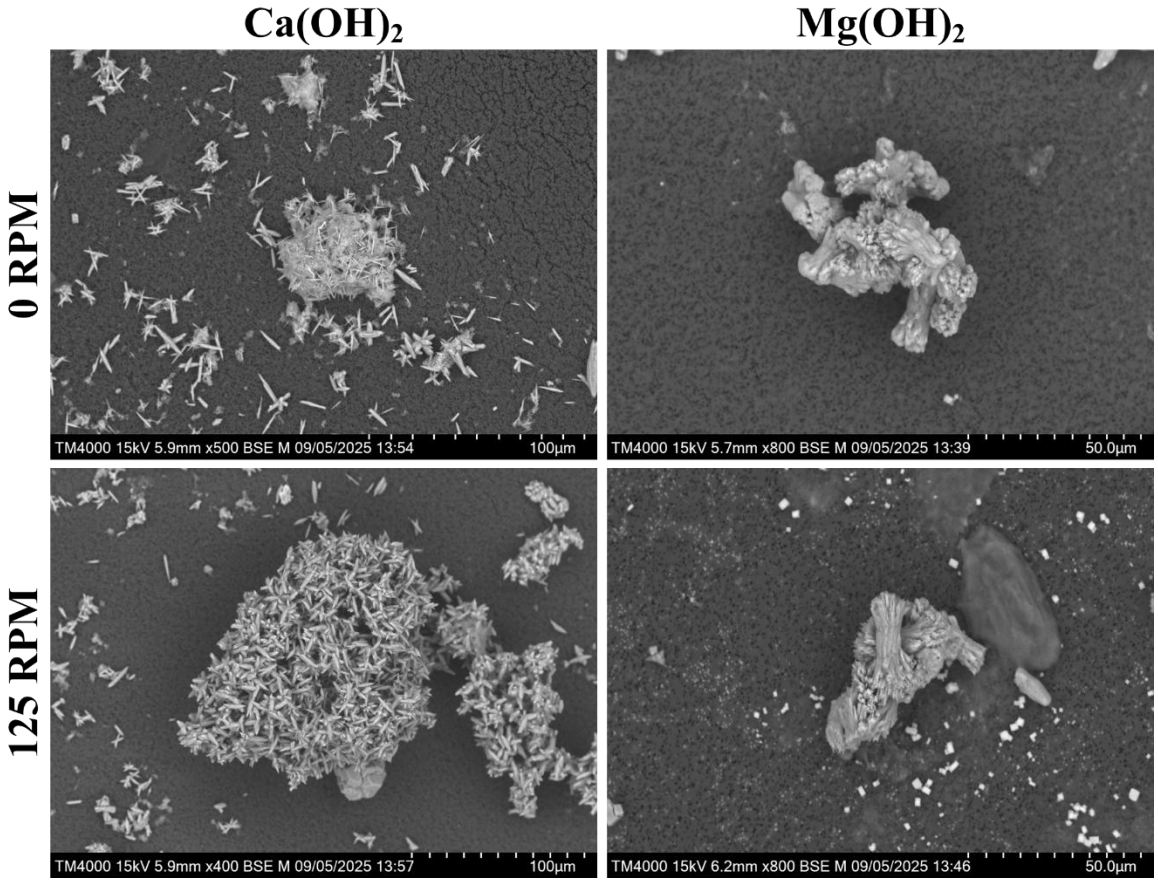

Figure 5: SEM images of precipitates collected from the experiments with higher additions of $Ca(OH)_2$ (left) and $Mg(OH)_2$ (right), both at 0RPM (top) and 125RPM (bottom).

Discussion

Advection affects alkaline material dissolution kinetics, $CaCO_3$ precipitation kinetics, and CO_2 ingassing rate

Considering real-world applications for OAE is of high interest but is yet to be fully addressed. In an effort to incorporate natural processes in laboratory experiments, the tests conducted here have deviated from the more classical experimental setup available in the literature and were conducted for an extended period of 6 months. The strong and rather unnatural stirring generated by a magnetic stir bar was traded for a more linear and mild approach using a shaking table. The role of CO_2 ingassing was also investigated. A very general observation regarding alkalinity generation is that the dissolution of such materials here was lower than reported in the literature (Hartmann et al., 2023; Moras et al., 2022; Moras et al., 2024;

https://doi.org/10.5194/egusphere-2025-6144
Preprint. Discussion started: 16 January 2026

Varliero et al., 2024; Yang et al., 2023). Such an outcome was to be expected as the milder, yet likely more realistic approach of the shaking table decreases the dissolution effect and disturbance created with a magnetic stir bar. The low (125RPM) or absent (0RPM) advection decreased the speed of diffusion around the particles. Hence, TA generation was up to 50% lower at 0RPM for the lower additions, due to the slower dissolution and higher saturation in the diffusive boundary layer. This suggests that solid-based OAE implementation should only be considered in environments with strong advection and/or disturbances.

This is also valid for NaOH-based OAE. While these incubations were only used as controls for the higher TA additions, a significant difference in TA generations was observed. Once exposed to advection, TA reached about 92% of the expected TA before increasing consistently to reach 100% on day 108 (Figure 4). The lack of TA generation at the start is likely due to secondary mineral formation, but unlikely in the form of $CaCO_3$. If it had been the case, a drop in DIC should have been observed early on, and no increase in TA later would have been expected due to the non-dissolution of $CaCO_3$ in seawater (Morse et al., 2007). Hence, the lack of TA generation had to come from the formation of a mineral that only affects TA and not $CaCO_3$, which is the case of $Mg(OH)_2$. $Mg(OH)_2$ precipitation following NaOH addition has been observed in the context of OAE, though at higher addition of NaOH (Hashim et al., 2025; Suitner et al., 2024; Varliero et al., 2024). In our experiments, the absence of advection likely led to $Mg(OH)_2$ precipitation, which ultimately redissolved over time. While these observations were not the focus of this study and therefore lack further analyses, they may have implications for OAE efficiency. While initially the loss of TA may lead to a temporary lower efficiency, it is later compensated by the redissolution of $Mg(OH)_2$, leading, in our case, to 100% of TA generation. However, the effect of advection is clearly noticeable in the 0RPM experiments. Maximum TA generated only reached about 330 µmol kg^{-1} on day 3 before decreasing. The concomitant decrease in DIC suggests $CaCO_3$ precipitation both after NaOH addition and in a runaway fashion during the first months (Figure 4). While $Mg(OH)_2$ likely precipitated as well, the further loss of TA and DIC in a runaway fashion, indicative of $CaCO_3$ formation, likely hid or undermined visible $Mg(OH)_2$ dissolution patterns.

Like in the NaOH experiments, $CaCO_3$ precipitation was suspected in the experiments with solid feedstocks. The creation of highly alkaline microenvironments led to inevitable secondary $CaCO_3$ precipitation. Furthermore, the low to inexistent advection led to longer CAP, allowing for more $CaCO_3$ to be formed. The presence of such saturated microenvironments, particularly in the diffusive boundary layer of dissolving particles, enhanced heterogeneous $CaCO_3$ precipitation on feedstock particles (Marion et al., 2009). In all experiments, $CaCO_3$ formation was suspected, with a clear decrease in DIC after addition in the 0RPM experiments, and a loss in DIC for all levels above 300 µmol kg^{-1} at 125RPM (Figure A 2). This was confirmed by SEM imaging (Figure 5) and particulate analysis (Table 1). While the measured particulate $CaCO_3$ only explained about 60% of the TA loss, likely from solid sticking to the bottle's wall, the data support the hypothesis that $CaCO_3$ formed on dissolving feedstock. The signal of Mg was twice as high in particles from the 0RPM experiments as in those of the 125RPM experiments. This likely resulted from coating of $Mg(OH)_2$ particles by $CaCO_3$, though it could not be successfully confirmed via SEM image. Hence, the lower TA generation in all experiments could be attributed to opposing mechanisms: the dissolution of alkaline minerals which increases TA, the loss of TA potential from the $CaCO_3$ coating of

https://doi.org/10.5194/egusphere-2025-6144
Preprint. Discussion started: 16 January 2026

such minerals, and the precipitation of $CaCO_3$, which decreases TA. While $CaCO_3$ precipitation has been well described in literature, a new external factor presented here makes the measurement of the rates harder. The continuous CO_2 ingassing occurring in all experiments maintains a positive increase in DIC over time. Measuring a decrease of TA and DIC in a 2:1 ratio would have given a good indication of $CaCO_3$ formation. Unfortunately, the CO_2 ingassing created from the added TA negates such a ratio as the loss of DIC from $CaCO_3$ is compensated by an increase from ingassing (Zeebe and Wolf-Gladrow, 2001).

Different observed $CaCO_3$ precipitation patterns and morphologies

A new $CaCO_3$ precipitation pattern emerged from the experiments with $Ca(OH)_2$ and $Mg(OH)_2$. $CaCO_3$ formation in the context of OAE has been described as a runaway process when using solid feedstocks, where the amount of alkalinity removed from the system is higher than the amount of alkalinity added. Here, such a process can be observed in most of the 0RPM experiments. However, the loss of alkalinity to $CaCO_3$ in the 125RPM differs. A linear and constant loss can be observed in the ΔTA +600 µmol kg^{-1} of the $Ca(OH)_2$ experiments, while for all the other 125RPM experiments, the early formation of $CaCO_3$ quickly stops after a few days of experiments. This unusual halt of precipitation is correlated with the quick increase in DIC following CO_2 ingassing. The duration of the CAP mentioned earlier is likely responsible for such a halt in the precipitation process.

Recent studies have identified thresholds for runaway $CaCO_3$ precipitation and have correlated its trigger to the time at which the CAP is maintained, Ω_A values, and surface area available (Suitner et al., 2025). Ultimately, the process stops at varying values of Ω_A, with similar experiments observing the stop to occur at Ω_A ~2 (Moras et al., 2022; Moras et al., 2024). Under such consideration, any process decreasing the CAP would decrease precipitation. One external factor not reported yet in the literature is the CO_2 ingassing. When CO_2 dissolves in water, Ω_A decreases due to the conversion of dissolved CO_2 and carbonate ions, CO_3^{2-}, into two bicarbonate ions, HCO_3^- (Zeebe and Wolf-Gladrow, 2001). Hence, the faster the CO_2 ingassing occurs, the less likely it is for $CaCO_3$ to precipitate in a runaway fashion. This is clearly visible here, where when a low CO_2 ingassing occurs, such as in the 0RPM experiments (Figure 3), the CAP is maintained for longer and $CaCO_3$ precipitates in a runaway fashion. When CO_2 quickly ingasses as in the 125RPM experiments, the duration of the CAP is significantly shorter, preventing $CaCO_3$ runaway precipitation. Under such considerations, OAE application should be considered in areas with higher CO_2 invasion rates to minimise the risks of $CaCO_3$ runaway precipitation (Figure 2, Figure 3).

Nevertheless, $CaCO_3$ formation likely occurred in all experiments (Figure A 2). DIC fluxes appear smaller between days 0 and 1 than between day 1 and 3 in the 100-300 µmol kg^{-1} additions at 125RPM, particularly with in the $Ca(OH)_2$ experiments. The discrepancy likely results from the concomitant DIC loss from $CaCO_3$ precipitation, and DIC increase from CO_2 ingassing. Such an assumption was confirmed by SEM analyses, where $CaCO_3$ crystals appeared in two distinctive morphologies and varied based on the alkaline material used. All crystal morphotypes identified were aragonite, which was expected given that they were formed in seawater, and EDS analyses did not reveal any significant incorporation of other

https://doi.org/10.5194/egusphere-2025-6144
Preprint. Discussion started: 16 January 2026

ions. Using $Ca(OH)_2$ resulted in needle-like aragonite crystals similar to those described in Moras et al. (2022). However, using $Mg(OH)_2$ resulted in spherulitic (broccoli-shaped) aragonite crystals, similar to those synthesised by Suitner et al. (2024). Synthesis of aragonite has been undertaken in a variety of experimental setups, with various factors such as varying Mg:Ca ratios and dissolved organic matter (Chave and Suess, 1970; Morse et al., 1997; Pan et al., 2021; Pytkowicz, 1965; Rushdi et al., 1992). Given that all experiments presented here were conducted in parallel and using the same batch of seawater, differences in the starting Mg:Ca ratio or dissolved organic matter concentration are negligible. However, the slower dissolution of $Mg(OH)_2$ compared to $Ca(OH)_2$ and its natural $CaCO_3$ inhibitory effect may be at play (Morse et al., 1997; Pan et al., 2021; Pytkowicz, 1965). In the context of slow-dissolving $Mg(OH)_2$ particles and the low (125RPM) or inexistent (0RPM) water movement on the particle surface, higher Ω_A and $[Mg^{2+}]$ in the diffusive boundary layers were maintained. Precipitation could therefore occur for longer while the inhibitory effect of Mg forced $CaCO_3$ to crystallise at a slower pace. Such conditions have been reported as favouring broccoli-shaped crystals over needle-like structures (Beck and Andreassen, 2010; Gránásy et al., 2005; Tracy et al., 1998; Zubovic et al., 2025).

Environmental implications of the decreased CAP

A primary outcome of this research is the impact of the CAP duration on various geochemical processes. This duration will also dictate potential environmental effects on organisms. It is important to note that any impact of OAE on biology does not result from alkalinity itself but rather the changes in carbonate chemistry following alkalinity addition (Bach et al., 2019). In fact, the depletion of dissolved CO_2 concentration and the increase in pH following alkalinity addition are responsible for the observed effects. Hence, the duration of the CAP will likely dictate how biology responds to alkalinity addition in an OAE context. Several studies have explored the impacts of OAE on biology, with a focus ranging from phytoplankton to fish larvae (Faucher et al., 2025; Ferderer et al., 2022; Ferderer et al., 2024; Goldenberg et al., 2024; Kousoulas et al., 2025; Paul et al., 2025; Ramírez et al., 2025). Generally, experiments conducted using an equilibrated approach, i.e., alkalinity increase occurring in parallel to DIC increase, resulting in low to negligible pH and pCO_2 changes, yielded mild to no changes (Kousoulas et al., 2025; Paul et al., 2025; Ramírez et al., 2025). Without depletion of the CO_2 concentration, organisms' response appeared mild to negligible in most cases, suggesting that equilibrated OAE is safer for implementation. However, using non-equilibrated approaches, i.e., with alkaline materials that only increase TA and not DIC, such as with $Ca(OH)_2$, $Mg(OH)_2$ and NaOH, may result in observable effects. In batch cultures, *Emiliania huxleyi* growth was not optimal when exposed to pCO_2 values below ~100 µatm following NaOH addition (Faucher et al., 2025). This is consistent with further research on the response of other key phytoplankton groups, i.e., diatoms, to OAE (Ferderer et al., 2024; Ferderer et al., 2025). There, the optimal growth of diatoms was estimated at pCO_2 values above ~120 µatm, where, once exposed to lower values, some negative effects could be observed.

However, these observations mostly occurred after days of experiments, which omitted CO_2 invasion in nearly all cases. The absence of CO_2 exchange with the atmosphere allowed for prolonged exposure to low pCO_2 conditions. Such a process would be less likely to occur in natural settings where CO_2 exchanges will take place as soon as alkalinity is released. One

https://doi.org/10.5194/egusphere-2025-6144
Preprint. Discussion started: 16 January 2026

can therefore argue that the quick invasion of CO_2 as observed in our experiments may decrease or even negate any effect of OAE on organisms' response. A mesocosms study reports that pCO_2 of ~250 µatm led to optimal coccolithophore calcification (Schneider et al., 2026). In our experiments with no advection, low pCO_2 conditions were observed over 1 week to 1 month, though pCO_2 only decreased down to ~200 µatm with NaOH (Figure 3, Figure 4). This suggests that under the carbonate chemistry conditions observed in our experiments, little to no effect would have been observed on the coccolithophores' response. Furthermore, once exposed to advection, the time of exposure to low pCO_2 levels decreased to a few days, with pCO_2 levels in all experiments promptly returning to background levels after up to 6 days. The decreased CAP led to limited maintenance of high pH and low CO_2 levels. The experiments presented here highlight that despite a CO_2 transfer velocity lower than the average in the open ocean (see below), the quick decrease of pH and rapid replenishment of dissolved CO_2 after alkalinity addition could efficiently decrease risks for living organisms. This is still largely overlooked in laboratory-scale experiments. Based on observations and assumptions made here, one could argue that OAE effects on biology in laboratory experiments without CO_2 exchanges serve as a lower limit. Hence, real-world OAE applications may only have small effects, if any, on living organisms.

Altered CDR potential of $Ca(OH)_2$ and $Mg(OH)_2$ and implication for MRV

$Ca(OH)_2$ and $Mg(OH)_2$ have appeared in several laboratory-scale studies and are among the minerals that have been strongly considered for OAE (Eisaman et al., 2023; Moras et al., 2022; Moras et al., 2024; Shaw et al., 2025; Varliero et al., 2024; Yang et al., 2023). From a thermodynamic point of view, both minerals generate 2 moles of TA per mole of mineral dissolved. Assuming the efficiency of 0.75 – 0.9 moles of CO_2 captured per mole of TA (Schulz et al., 2023), $Ca(OH)_2$ would allow for 0.9 – 1.1 tonne of CO_2 per tonne of $Ca(OH)_2$, and $Mg(OH)_2$ would allow for 1.1 – 1.4 tonne of CO_2 per tonne of $Mg(OH)_2$. Such potential is already decreased if, for example, the CO_2 emitted during the calcination of limestone to produce $Ca(OH)_2$ is not captured (Caserini et al., 2021; Foteinis et al., 2022; Kheshgi, 1995). Another CDR potential pitfall using either of these hydroxides is the incomplete TA generation presented here. With a theoretical safe OAE implementation, where only a low amount of alkalinity was to be added, e.g., 100 µmol kg^{-1} (Bach et al., 2025), and exposed to some advection, e.g., 125RPM, the actual realised TA only reaches 55-58% (Figure 1). The competing processes of CO_2 ingassing and $CaCO_3$ precipitation make the actual measurement of TA generation complicated, as the DIC usually used to decipher between incomplete mineral dissolution and $CaCO_3$ precipitation is not suitable when CO_2 ingassing is allowed in the system. This is therefore true if OAE were to be implemented in the ocean, and there are major unknowns for monitoring, reporting and verification (MRV) protocols. Despite high-quality measurement instruments, competing processes likely hide the impacts of each other and increase overall measurement uncertainties, as highlighted by the large standard error from these experiments (Figure 2, Figure 3, Figure 4, Figure A 2, Figure A 3).

$CaCO_3$ precipitation is undoubtedly a major pitfall for MRV protocols for OAE, as it decreases its overall CDR potential and may lead to unwanted seawater changes (Moras et al., 2022). While it may occur both with particulate and liquid feedstocks, as well as in both equilibrated and unequilibrated approaches, the fate of the precipitates is still hard to comprehend and

https://doi.org/10.5194/egusphere-2025-6144
Preprint. Discussion started: 16 January 2026

safely report on. A general assumption is that, given the oversaturation of seawater with respect to aragonite, any precipitated aragonite crystal will not dissolve in natural open ocean surface water (Morse et al., 2007). Hence, the crystals will ultimately sink and be transported to the deeper ocean (Suitner et al., 2025). The removal of surface area in the surface layer may prevent further precipitation and will not decrease the CDR potential significantly. Once transported in the deeper waters, $CaCO_3$ particles may redissolve in areas of undersaturated seawater or be buried in sediments without further dissolution (Dale et al., 2024; Fuhr et al., 2025). Since $CaCO_3$ precipitation mostly occurred on added particles, as explained earlier, another loss in CDR potential results from the coating of alkaline feedstock particles and their inevitable removal from the surface layer via sinking. It is acknowledged, though, that in bottle experiments, the sinking of $CaCO_3$ does not happen, which leads to a higher load of surface area remaining available for further precipitation to occur.

Yet, the persistence of alkaline material in the surface layer is a prerequisite for higher CDR potential. Hence, sinking of particles needs to be thoroughly understood, and coupling $CaCO_3$ formation rates with sinking speed is yet to be addressed. Residence times of particles in the surface layer of the ocean are directly correlated with the size and density of particles (Suitner et al., 2025). Using modelling considerations from Suitner et al. (2025), one could hypothesise that the amount of $Ca(OH)_2$ coated by needle-like $CaCO_3$, if any, is negligible or will be fully dissolved as their uneven formation allows for water to seep between the needle structures and reach undissolved $Ca(OH)_2$. However, the persistence of such needles in the surface layer for weeks to months may offer surface area for longer times and allow for $CaCO_3$ precipitation to occur later on. Using $Mg(OH)_2$ particles would lead to the opposite. Given that the slower dissolving $Mg(OH)_2$ allows for a higher CAP in the diffusive boundary layer, coating of such particles may occur more efficiently, resulting in a loss of TA generation. Because $CaCO_3$ appeared to be formed as broccoli-shaped structures, these larger structures present a higher sinking velocity and may quickly transport undissolved $Mg(OH)_2$ out of the surface layer. But the quick sinking occurring within days may be sufficient to significantly decrease the available surface area for further precipitation, limiting the loss of TA to $CaCO_3$. These statements are only hypotheses and require further work.

Linking laboratory data with modelling studies and future OAE research

Current understandings of the global CDR potential of OAE mostly rely on models and rarely implement laboratory experiment results. Correlating results obtained in bottle experiments with global modelling remains largely overlooked and is still a major shortcoming in OAE research. Using the DIC fluxes and pCO_2 data collected in these experiments, a first attempt to put ours into modelling studies context can be undertaken. Using the first steps after alkalinity addition, i.e., between days 1 and 3, DIC increases were 21.3 ±14.3 and 39.9 ±25.3 μmol kg^{-1} d^{-1} for the 0 and 125RPM experiments, respectively. Large uncertainties mostly arise from $CaCO_3$ precipitation that occurred at varying rates based on the mineral and the amount added. Yet, using those data and the difference in pCO_2 between background and seawater at day 1, an estimate of the gas transfer velocity k (in cm h^{-1}) can be derived and compared to natural systems using the air-sea gas fluxes equation (Wanninkhof, 2014):

https://doi.org/10.5194/egusphere-2025-6144
Preprint. Discussion started: 16 January 2026

$$F = kK_0(pCO_{2w} - pCO_{2a})$$

where F is the flux of CO_2 between the atmosphere and the bottle between day 1 and 3, expressed in mol m^{-2} d^{-1}, K_0 is the solubility of CO_2 in seawater (obtained from Weiss (1974), estimated at $2.932.10^{-2}$ mol L^{-1} atm^{-1} at 24.6 °C and for a salinity of 35.4 in our experiments), and pCO_{2w} and pCO_{2a}, the partial pressures of the seawater and air in atm, respectively, at day 1 following alkalinity addition. Given that F, K_0 and the pCO_2 difference are known, as well as the depth of the water at day 3, i.e., ~10.5 cm, and the density of seawater of salinity 35.346 at 24.6 °C (Millero and Poisson, 1981), the gas velocities for the 0RPM and 125RPM experiments can be estimated, i.e., k_{0RPM} and k_{125RPM}, respectively (the authors emphasize that even though these may not fully reflect natural conditions, they provide a first useful initial approximation).

k_{0RPM} was estimated at 1.4 ±0.6 cm h^{-1}, while exposing the bottles to an advection speed of 125RPM led to a k_{125RPM} of 2.7 ±1.1 cm h^{-1}. These gas velocities are significantly lower than those observed naturally in the open ocean but may be correlated to wind speed. Estimates of the corresponding wind speed in our experiments can be derived from the gas exchange wind speed relationship from Wanninkhof (2014):

$$k = 0.251\, U^2 \left(\frac{Sc}{660}\right)^{-0.5}$$

where U^2 is the wind speed at 10m height in m s^{-1}, and Sc is the Schmidt number at 24.6 °C and salinity 35. Resolving this equation at 24.6 °C corresponds then to wind speeds of about 2.2 m s^{-1} and 3.1 m s^{-1} for the 0 and 125RPM experiments, respectively. Wind speed in the open ocean varies greatly, from less than 1 m s^{-1} to over 20 m s^{-1} during heavy wind and storm periods, averaging ~6 m s^{-1} (Ho et al., 2006; Miller et al., 2010; Risien and Chelton, 2008). Hence, the data presented here can be compared to low to moderate wind scenarios and be used for modelling in specific geographical areas, mostly around the Equator (Tokinaga and Xie, 2011).

Geographical areas where lower wind speeds are observed mostly coincide with lower wave heights (Tokinaga and Xie, 2011). While the effect of wave height on the dissolution of alkaline materials is not well understood, one could assume that the stronger the water movement and disturbance, the quicker the dissolution, though it is purely hypothetical here. Our data would then represent the lower end of OAE application. Also, given that surface water subduction speed is not correlated to wave height, alkaline surface water may remain in contact with the atmosphere for longer (Cushman-Roisin and Beckers, 2011). Hence, regions with stronger winds and higher waves may allow for faster mineral dissolution and CO_2 ingassing rates than presented here. That also suggests that $CaCO_3$ precipitation from microenvironments may occur less likely, or at least not as fast. Implementing the data presented here in a global model may yield lower overall CDR estimates, but most likely conservative rates, which can therefore serve as a base for further work and considerations in MRV protocols.

https://doi.org/10.5194/egusphere-2025-6144
Preprint. Discussion started: 16 January 2026

Conclusion

The experiments presented here report on the first long-term (6 months) laboratory incubations for OAE. Varying alkalinity increases using $Ca(OH)_2$, $Mg(OH)_2$ and NaOH were targeted in stagnant and in advected seawater. A first important outcome was the lower measured TA compared to the expected one. Maximums of ~20-30% at 0RPM and ~60% at 125RPM of expected TA were measured following low alkalinity additions, before decreasing down to less than 10% at 0RPM and ~10-35% at 125RPM. All experiments with solid feedstocks revealed $CaCO_3$ precipitation, with more formation occurring without motion. $CaCO_3$ formation was directly correlated to the amount of $Mg(OH)_2$ added at 125RPM, while past a threshold of 300 µmol kg^{-1} using $Ca(OH)_2$, the TA generation decreased, and $CaCO_3$ precipitation rate increased at 125RPM. Precipitated $CaCO_3$ particles did not redissolve during the 6-month experiments. Using NaOH revealed co-precipitation of $CaCO_3$ and $Mg(OH)_2$ at 0RPM, which did not redissolve, yielding a maximum TA generation of ~55%, while at 125RPM, $CaCO_3$ was negligible if any, and the early $Mg(OH)_2$ eventually dissolved after 3 months, leading to 100% of the TA release. $CaCO_3$ precipitation occurred in two distinct morphologies based on the solid feedstock used. Needle-like aragonite crystals formed with $Ca(OH)_2$, while broccoli-shaped aragonite was formed with $Mg(OH)_2$, most likely coating $Mg(OH)_2$ particles. In real ocean applications, the permanence of the needle-like structure in the surface layer may trigger further $CaCO_3$ precipitation, while the sinking of broccoli-like crystals would remove surface area for further precipitation in the surface layer. Finally, the 125RPM experiments corresponded to open ocean wind speeds of about 3.1 m s^{-1}, about half of the average open ocean wind speeds. The patterns presented here may be significantly decreased as stronger CO_2 ingassing rates in the open ocean will limit the persistence of the CAP around particles. Thus, this may not significantly impact the overall CDR potential of OAE, while the quick CO_2 ingassing will allow for a fast decrease in pH and replenishing of the CO_2 concentration after alkalinity addition, decreasing side effects on living organisms.

https://doi.org/10.5194/egusphere-2025-6144
Preprint. Discussion started: 16 January 2026

Appendix A

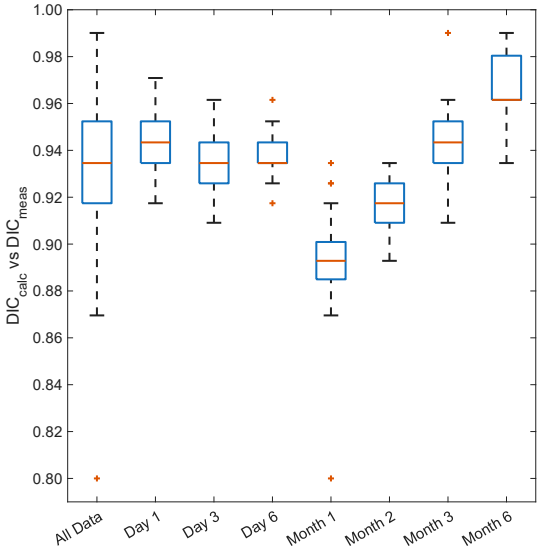

Figure A 1: Boxplots of the ratio between the calculated DIC from TA and pH_T data and the measured DIC for all compiled data, and as a function of the dataset analysed. The boxplots from the month 1 and 2 datasets clearly fall below the boxplot of the ratios of the compiled data, while the month 6 data stands above the boxplot of the ratios of the compiled data.

https://doi.org/10.5194/egusphere-2025-6144
Preprint. Discussion started: 16 January 2026

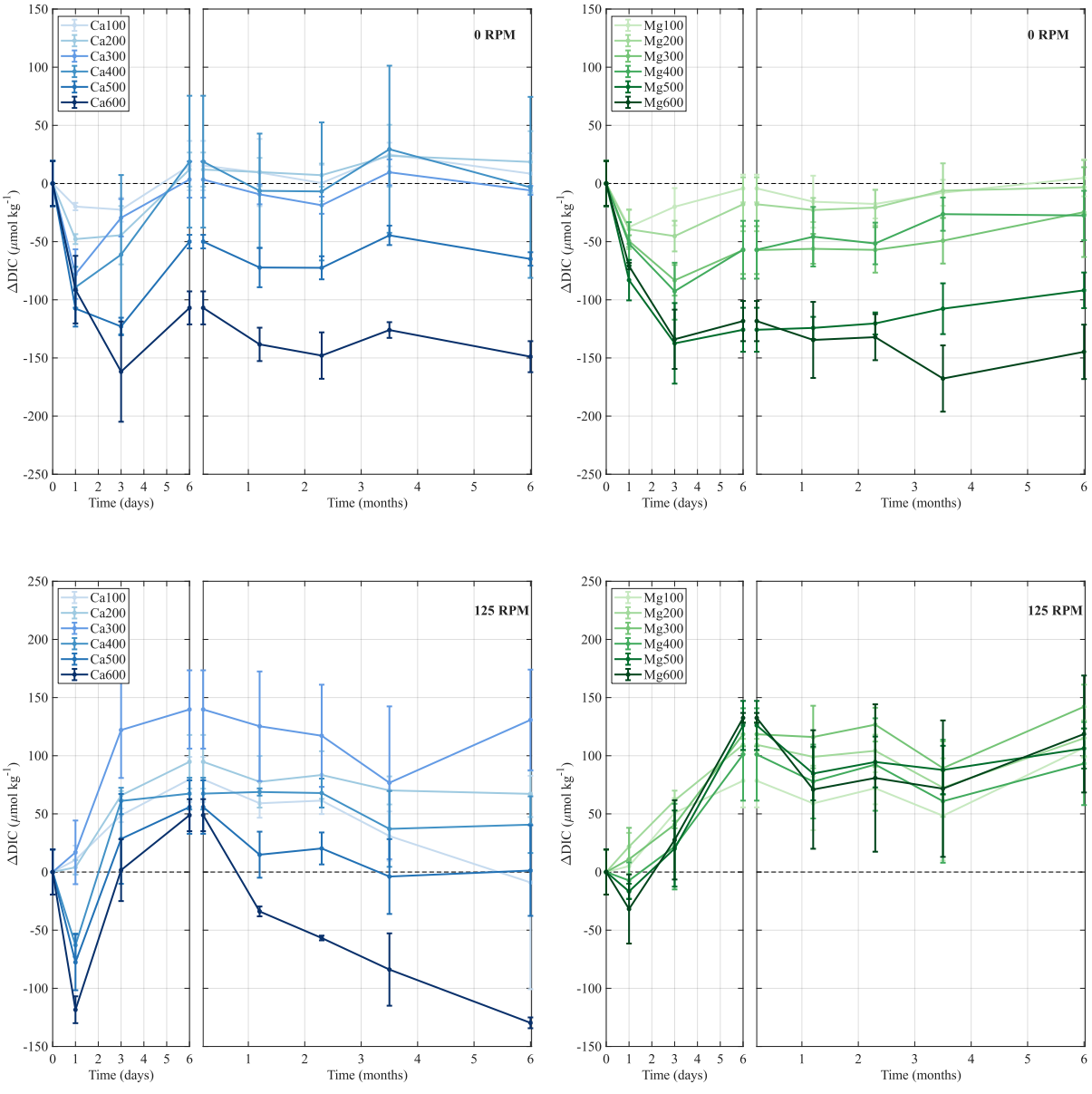

Figure A 2: Changes in ΔDIC over time following $Ca(OH)_2$ (blue) or $Mg(OH)_2$ (green) additions with 0RPM (top) and 125RPM advection (bottom) advection. The darker shades indicate higher alkaline material additions. Each point represents the average of triplicates, with ranges representing the uncertainty based on the standard deviation of these three measurements.

https://doi.org/10.5194/egusphere-2025-6144
Preprint. Discussion started: 16 January 2026

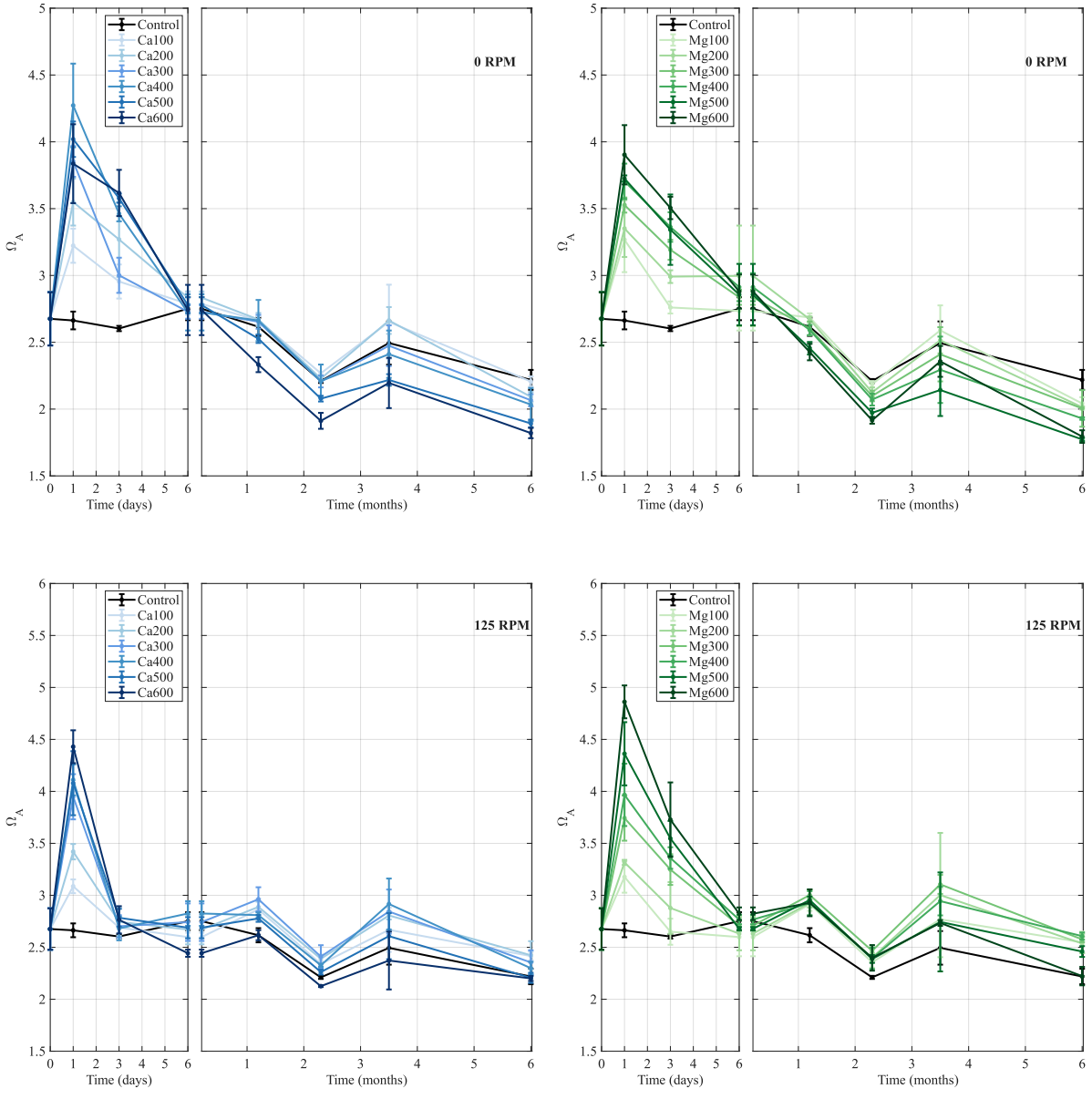

525 **Figure A 3: Changes in Ω_A over time following $Ca(OH)_2$ (blue) or $Mg(OH)_2$ (green) additions with 0RPM (top) and 125RPM advection (bottom) advection. The darker shades indicate higher alkaline material additions. Each point represents the average of triplicates, with ranges representing the uncertainty based on the standard deviation of these three measurements.**

https://doi.org/10.5194/egusphere-2025-6144
Preprint. Discussion started: 16 January 2026

Data Availability

The data will be made available in a public repository upon acceptance of the manuscript for publication.

Author Contribution

CAM designed the experiments with inputs from JH. CAM and MSM ran the experiments. CAM and PB performed the analyses. CAM wrote the first draft of the manuscript, and inputs from JH, as well as further inputs from MSM and PB, led to the final version of the manuscript.

Competing Interests

JH is consulting for the Planeteers GmbH. All authors declare that they have no competing interests.

Acknowledgments

The authors would like to thank Prof. Douglas Wallace from Dalhousie University, Canada, for his early advice on the experimental setup, Assoc. Prof. Ruth Musgrave for her inputs on gas velocity calculations, and the broader Ocean Alk-align team for their inputs during online meetings. The authors would also like to thank Dr Niko Lahajnar for accommodating laboratory space, as well as Dr Dirk Eifler and Nuray Eroglu for their support with F-AAS analyses. The authors acknowledge the use of AI for literature search. All relevant output was subsequently checked and reviewed before consideration for in-text incorporation by the authors.

Financial Support

This research has been supported by the Ocean Alk-Align project funded by the Carbon to Sea Initiative, and by the German Federal Ministry of Education and Research through the CDRmare project RETAKE-II (grant no 03F0965F).

https://doi.org/10.5194/egusphere-2025-6144
Preprint. Discussion started: 16 January 2026

References

Bach, L. T., Tyka, M. D., Wang, B., and Fennel, K.: Lethal by design? Guiding environmental assessments of ocean alkalinity enhancement toward realistic contextualization of the alkalinity perturbation, CDRXIV, 10.70212/cdrxiv.2025457.v1, 2025.

Bach, L. T., Gill, S. J., Rickaby, R. E. M., Gore, S., and Renforth, P.: CO_2 removal with enhanced weathering and Ocean Alkalinity Enhancement: Potential risks and co-benefits for marine pelagic ecosystems, Frontiers in Climate, 1, 10.3389/fclim.2019.00007, 2019.

Badocco, D., Pedrini, F., Pastore, A., di Marco, V., Marin, M. G., Bogialli, S., Roverso, M., and Pastore, P.: Use of a simple empirical model for the accurate conversion of the seawater pH value measured with NIST calibration into seawater pH scales, Talanta, 225, 122051, j.talanta.2020.122051, 2021.

Beck, R. and Andreassen, J.-P.: Spherulitic Growth of Calcium Carbonate, Crystal Growth & Design, 10, 2934-2947, 10.1021/cg901460g, 2010.

Caserini, S., Pagano, D., Campo, F., Abbà, A., De Marco, S., Righi, D., Renforth, P., and Grosso, M.: Potential of maritime transport for ocean liming and atmospheric CO_2 removal, Frontiers in Climate, 3, 10.3389/fclim.2021.575900, 2021.

Chave, K. E. and Suess, E.: Calcium carbonate saturation in seawater: Effects of dissolved organic matter, Limnology and Oceanography, 15, 633-637, 10.4319/lo.1970.15.4.0633, 1970.

Cushman-Roisin, B. and Beckers, J.-M.: Chapter 20 - Oceanic General Circulation, in: International Geophysics, edited by: Cushman-Roisin, B., and Beckers, J.-M., Academic Press, 657-699, 10.1016/B978-0-12-088759-0.00020-1, 2011.

Dale, A. W., Geilert, S., Diercks, I., Fuhr, M., Perner, M., Scholz, F., and Wallmann, K.: Seafloor alkalinity enhancement as a carbon dioxide removal strategy in the Baltic Sea, Communications Earth & Environment, 5, 452, 10.1038/s43247-024-01569-3, 2024.

Dickson, A. G.: Standard potential of the reaction: $AgCl(s) + 12H_2(g) = Ag(s) + HCl(aq)$, and the standard acidity constant of the ion HSO_4^- in synthetic sea water from 273.15 to 318.15 K, The Journal of Chemical Thermodynamics, 22, 113-127, 10.1016/0021-9614(90)90074-Z, 1990.

Dickson, A. G.: Standards for ocean measurements, Oceanography, 23, 34-47, 10.5670/oceanog.2010.22, 2010.

Dickson, A. G., Sabine, C. L., and Christian, J. R.: Guide to best practices for ocean CO_2 measurements, PICES Special Publication 3; IOCCP Report 8, Sidney, British Columbia, North Pacific Marine Science Organization, 191 pp., 10.25607/OBP-1342, 1897176074, 2007.

Eisaman, M. D., Geilert, S., Renforth, P., Bastianini, L., Campbell, J., Dale, A. W., Foteinis, S., Grasse, P., Hawrot, O., Löscher, C. R., Rau, G. H., and Rønning, J.: Assessing the technical aspects of ocean-alkalinity-enhancement approaches, Guide to Best Practices in Ocean Alkalinity Enhancement Research, 2-oae2023, 3, 10.5194/sp-2-oae2023-3-2023, 2023.

Faucher, G., Haunost, M., Paul, A. J., Tietz, A. U. C., and Riebesell, U.: Growth response of Emiliania huxleyi to ocean alkalinity enhancement, Biogeosciences, 22, 405-415, 10.5194/bg-22-405-2025, 2025.

Ferderer, A., Chase, Z., Kennedy, F., Schulz, K. G., and Bach, L. T.: Assessing the influence of ocean alkalinity enhancement on a coastal phytoplankton community, Biogeosciences, 19, 5375-5399, 10.5194/bg-19-5375-2022, 2022.

Ferderer, A., Schulz, K. G., Riebesell, U., Baker, K. G., Chase, Z., and Bach, L. T.: Investigating the effect of silicate- and calcium-based ocean alkalinity enhancement on diatom silicification, Biogeosciences, 21, 2777-2794, 10.5194/bg-21-2777-2024, 2024.

Ferderer, A., Schulz, K. G., Willis, A., Baker, K. G., Chase, Z., and Bach, L. T.: Carbonate chemistry fitness landscapes inform diatom resilience to future perturbations, Science Advances, 11, eadu8024, doi:10.1126/sciadv.adu8024, 2025.

Foteinis, S., Andresen, J., Campo, F., Caserini, S., and Renforth, P.: Life cycle assessment of ocean liming for carbon dioxide removal from the atmosphere, Journal of Cleaner Production, 370, 133309, 10.1016/j.jclepro.2022.133309, 2022.

https://doi.org/10.5194/egusphere-2025-6144
Preprint. Discussion started: 16 January 2026

Fuhr, M., Dale, A. W., Wallmann, K., Bährle, R., Kalapurakkal, H. T., Sommer, S., Spiegel, T., Dobashi, R., Buchholz, B., Schmidt, M., Perner, M., and Geilert, S.: Calcite is an efficient and low-cost material to enhance benthic weathering in shelf sediments of the Baltic Sea, Communications Earth & Environment, 6, 106, 10.1038/s43247-025-02079-6, 2025.

Goldenberg, S. U., Riebesell, U., Brüggemann, D., Börner, G., Sswat, M., Folkvord, A., Couret, M., Spjelkavik, S., Sánchez, N., Jaspers, C., and Moyano, M.: Early life stages of fish under ocean alkalinity enhancement in coastal plankton communities, Biogeosciences, 21, 4521-4532, 10.5194/bg-21-4521-2024, 2024.

Gránásy, L., Pusztai, T., Tegze, G., Warren, J. A., and Douglas, J. F.: Growth and form of spherulites, Physical Review E, 72, 011605, 10.1103/PhysRevE.72.011605, 2005.

Hartmann, J., Suitner, N., Lim, C., Schneider, J., Marín-Samper, L., Arístegui, J., Renforth, P., Taucher, J., and Riebesell, U.: Stability of alkalinity in ocean alkalinity enhancement (OAE) approaches – consequences for durability of CO_2 storage, Biogeosciences, 20, 781-802, 10.5194/bg-20-781-2023, 2023.

Hashim, M. S., Marx, L., Klein, F., Dean, C. L., Burdige, E., Hayden, M., McCorkle, D. C., and Subhas, A. V.: Mineral formation during shipboard ocean alkalinity enhancement experiments in the North Atlantic, Biogeosciences, 22, 7149-7165, 10.5194/bg-22-7149-2025, 2025.

Hausfather, Z.: An assessment of current policy scenarios over the 21st century and the reduced plausibility of high-emissions pathways, Dialogues on Climate Change, 2, 26-32, 10.1177/29768659241304854, 2025.

Ho, D. T., Law, C. S., Smith, M. J., Schlosser, P., Harvey, M., and Hill, P.: Measurements of air-sea gas exchange at high wind speeds in the Southern Ocean: Implications for global parameterizations, Geophysical Research Letters, 33, 10.1029/2006GL026817, 2006.

IPCC: Summary for Policymakers. In: Climate Change 2022: Impacts, Adaptation and Vulnerability. Contribution of Working Group II to the Sixth Assessment Report of the Intergovernmental Panel on Climate Change [H.-O. Pörtner, D.C. Roberts, M. Tignor, E.S. Poloczanska, K. Mintenbeck, A. Alegría, M. Craig, S. Langsdorf, S. Löschke, V. Möller, A. Okem, B. Rama (eds.)], Cambridge University Press, Cambridge, United Kingdom and New York, NY, USA, 2022.

Kheshgi, H. S.: Sequestering atmospheric carbon dioxide by increasing ocean alkalinity, Energy, 20, 915-922, 10.1016/0360-5442(95)00035-F, 1995.

Kousoulas, K., Ferderer, A., Eriksen, R., and Bach, L. T.: Winners and losers under hydroxide-based ocean alkalinity enhancement in a Tasmanian plankton community, Journal of Phycology, 61, 989-1006, 10.1111/jpy.70052, 2025.

Lee, K., Kim, T.-W., Byrne, R. H., Millero, F. J., Feely, R. A., and Liu, Y.-M.: The universal ratio of boron to chlorinity for the North Pacific and North Atlantic oceans, Geochimica et Cosmochimica Acta, 74, 1801-1811, 10.1016/j.gca.2009.12.027, 2010.

Lewis, E. L. and Perkin, R. G.: The practical salinity scale 1978: conversion of existing data, Deep Sea Research Part A. Oceanographic Research Papers, 28, 307-328, 10.1016/0198-0149(81)90002-9, 1981.

Marion, G. M., Millero, F. J., and Feistel, R.: Precipitation of solid phase calcium carbonates and their effect on application of seawater S_A - T - P models, Ocean Science, 5, 285-291, 10.5194/os-5-285-2009, 2009.

Miller, S. D., Marandino, C., and Saltzman, E. S.: Ship-based measurement of air-sea CO2 exchange by eddy covariance, Journal of Geophysical Research: Atmospheres, 115, 10.1029/2009JD012193, 2010.

Millero, F. J. and Poisson, A.: International one-atmosphere equation of state of seawater, Deep Sea Research Part A. Oceanographic Research Papers, 28, 625-629, 10.1016/0198-0149(81)90122-9, 1981.

Moras, C. A.: Assessing the dissolution of various crushed rocks and minerals for ocean alkalinity enhancement, Southern Cross University, 10.25918/thesis.332, 2023.

Moras, C. A., Bach, L. T., Cyronak, T., Joannes-Boyau, R., and Schulz, K. G.: Ocean alkalinity enhancement – avoiding runaway $CaCO_3$ precipitation during quick and hydrated lime dissolution, Biogeosciences, 19, 3537-3557, 10.5194/bg-19-3537-2022, 2022.

Moras, C. A., Bach, L. T., Cyronak, T., Joannes-Boyau, R., and Schulz, K. G.: Preparation and quality control of in-house reference materials for marine dissolved inorganic carbon and total alkalinity measurements, Limnology and Oceanography: Methods, 10.1002/lom3.10570, 2023.

https://doi.org/10.5194/egusphere-2025-6144
Preprint. Discussion started: 16 January 2026

Moras, C. A., Cyronak, T., Bach, L. T., Joannes-Boyau, R., and Schulz, K. G.: Effects of grain size and seawater salinity on magnesium hydroxide dissolution and secondary calcium carbonate precipitation kinetics: implications for ocean alkalinity enhancement, Biogeosciences, 21, 3463-3475, 10.5194/bg-21-3463-2024, 2024.

Morse, J. W., Arvidson, R. S., and Lüttge, A.: Calcium carbonate formation and dissolution, Chemical Reviews, 107, 342-381, 10.1021/cr050358j, 2007.

Morse, J. W., Wang, Q., and Tsio, M. Y.: Influences of temperature and Mg:Ca ratio on $CaCO_3$ precipitates from seawater, Geology, 25, 85-87, 10.1130/0091-7613(1997)025<0085:Iotamc>2.3.Co;2, 1997.

Pan, Y., Li, Y., Ma, Q., He, H., Wang, S., Sun, Z., Cai, W.-J., Dong, B., Di, Y., Fu, W., and Chen, C.-T. A.: The role of Mg^{2+} in inhibiting $CaCO_3$ precipitation from seawater, Marine Chemistry, 237, 104036, 10.1016/j.marchem.2021.104036, 2021.

Paul, A. J., Haunost, M., Goldenberg, S. U., Hartmann, J., Sánchez, N., Schneider, J., Suitner, N., and Riebesell, U.: Ocean alkalinity enhancement in an open-ocean ecosystem: biogeochemical responses and carbon storage durability, Biogeosciences, 22, 2749-2766, 10.5194/bg-22-2749-2025, 2025.

Perez, F. F. and Fraga, F.: Association constant of fluoride and hydrogen ions in seawater, Marine Chemistry, 21, 161-168, 10.1016/0304-4203(87)90036-3, 1987.

Pytkowicz, R. M.: Rates of inorganic calcium carbonate nucleation, The Journal of Geology, 73, 196-199, 10.1086/627056, 1965.

Ramírez, L., Pozzo-Pirotta, L. J., Trebec, A., Manzanares-Vázquez, V., Díez, J. L., Arístegui, J., Riebesell, U., Archer, S. D., and Segovia, M.: Ocean alkalinity enhancement (OAE) does not cause cellular stress in a phytoplankton community of the subtropical Atlantic Ocean, Biogeosciences, 22, 1865-1886, 10.5194/bg-22-1865-2025, 2025.

Risien, C. M. and Chelton, D. B.: A Global Climatology of Surface Wind and Wind Stress Fields from Eight Years of QuikSCAT Scatterometer Data, Journal of Physical Oceanography, 38, 2379-2413, 10.1175/2008JPO3881.1, 2008.

Rushdi, A. I., Pytkowicz, R. M., Suess, E., and Chen, C. T.: The effects of magnesium-to-calcium ratios in artificial seawater, at different ionic products, upon the induction time, and the mineralogy of calcium carbonate: A laboratory study, Geologische Rundschau, 81, 571-578, 10.1007/BF01828616, 1992.

Schneider, J., Riebesell, U., Moras, C. A., Marín-Samper, L., Kittu, L. R., Ortíz-Cortes, J., and Schulz, K. G.: Carbon fixation of a temperate plankton community in response to calcium- and silicate-based Ocean Alkalinity Enhancement using air-sea gas exchange measurements, Biogeosciences, 23, 137-153, 10.5194/bg-23-137-2026, 2026.

Schockman, K. M. and Byrne, R. H.: Spectrophotometric determination of the bicarbonate dissociation constant in seawater, Geochimica et Cosmochimica Acta, 300, 231-245, 10.1016/j.gca.2021.02.008, 2021.

Schulz, K. G., Bach, L. T., and Dickson, A. G.: Seawater carbonate system considerations for ocean alkalinity enhancement research, State Planet Discuss., 2023, 1-24, 10.5194/sp-2023-12, 2023.

Shaw, C., Ringham, M. C., Carter, B. R., Tyka, M. D., and Eisaman, M. D.: Using magnesium hydroxide for ocean alkalinity enhancement: elucidating the role of formation conditions on material properties and dissolution kinetics, Frontiers in Climate, Volume 7 - 2025, 10.3389/fclim.2025.1616362, 2025.

Suitner, N., Hartmann, J., Varliero, S., Faucher, G., Suessle, P., and Moras, C. A.: Surface area and Ω-aragonite oversaturation as controls of the runaway precipitation process in ocean alkalinity enhancement, EGUsphere, 2025, 1-26, 10.5194/egusphere-2025-381, 2025.

Suitner, N., Faucher, G., Lim, C., Schneider, J., Moras, C. A., Riebesell, U., and Hartmann, J.: Ocean alkalinity enhancement approaches and the predictability of runaway precipitation processes: results of an experimental study to determine critical alkalinity ranges for safe and sustainable application scenarios, Biogeosciences, 21, 4587-4604, 10.5194/bg-21-4587-2024, 2024.

Tang, H., Wu, X., Xian, H., Zhu, J., Wei, J., Liu, H., and He, H.: Heterogeneous nucleation and growth of $CaCO_3$ on calcite (104) and aragonite (110) surfaces: Implications for the formation of abiogenic carbonate cements in the ocean, Minerals, 10, 294, 10.3390/min10040294, 2020.

Tokinaga, H. and Xie, S.-P.: Wave- and Anemometer-Based Sea Surface Wind (WASWind) for Climate Change Analysis, Journal of Climate, 24, 267-285, 10.1175/2010JCLI3789.1, 2011.

Tracy, S. L., Williams, D. A., and Jennings, H. M.: The growth of calcite spherulites from solution: II. Kinetics of formation, Journal of Crystal Growth, 193, 382-388, 10.1016/S0022-0248(98)00521-1, 1998.

https://doi.org/10.5194/egusphere-2025-6144
Preprint. Discussion started: 16 January 2026

Varliero, S., Buono, A., Caserini, S., Raos, G., and Macchi, P.: Chemical Aspect of Ocean Liming for CO2 Removal: Dissolution Kinetics of Calcium Hydroxide in Seawater, ACS Engineering Au, 4, 422-431, 10.1021/acsengineeringau.4c00008, 2024.

Wanninkhof, R.: Relationship between wind speed and gas exchange over the ocean revisited, Limnology and Oceanography: Methods, 12, 351-362, 10.4319/lom.2014.12.351, 2014.

Weiss, R. F.: Carbon dioxide in water and seawater: the solubility of a non-ideal gas, Marine Chemistry, 2, 203-215, 10.1016/0304-4203(74)90015-2, 1974.

Yang, B., Leonard, J., and Langdon, C.: Seawater alkalinity enhancement with magnesium hydroxide and its implication for carbon dioxide removal, Marine Chemistry, 253, 104251, 10.1016/j.marchem.2023.104251, 2023.

Zeebe, R. E. and Wolf-Gladrow, D.: CO_2 in seawater: equilibrium, kinetics, isotopes, 65, Gulf Professional Publishing, 360 pp.0-444-50946-1, 2001.

Zubovic, K. P., Horvath, A., Brien, D. M., Rateau, R., Terribili, L., Winters, S., Docaigne, E., Guyett, P. C., and Rodriguez-Blanco, J. D.: Crystallisation of CaCO3 polymorphs induced by layered PET-based microplastic particles, Environmental Sciences Europe, 37, 52, 10.1186/s12302-025-01090-0, 2025.